

Numerical investigations on wavelength-tunable and bandwidth-controllable chaotic signal generation based on a WRC-FPLD subject to FBG filtered feedback

CHUN-XIA HU^{a,b}, GUANG-QIONG XIA^a, TAO DENG^a, ELUMALAI JAYAPRASATH^a, ZAI-FU JIANG^a, WEN-YAN YANG^{a,c}, ZHENG-MAO WU^{a,*}

^a*School of Physics, Southwest University, Chongqing 400715, China*

^b*College of Mobile Telecommunications Chongqing University of Posts and Telecom, Chongqing 401520, China*

^c*School of Mathematics and Physics, Chongqing University of Science and Technology, Chongqing 401331, China*

In this paper, we propose a modified multi-mode rate equation model to numerically study the chaotic dynamics of a weak resonant-cavity Fabry-Perot laser diode (WRC-FPLD) subject to fiber Bragg grating (FBG) feedback. The simulated results show that, by adjusting the Bragg wavelength of FBG, different longitudinal mode of the WRC-FPLD can be chosen to become a lasing mode. Under suitable feedback strength, such a lasing mode can operate at a chaotic state, and the bandwidth of the chaotic signal increases firstly and then decreases with the increase of k , which is consistent with our previously reported experimental results. Furthermore, the influences of the reflected bandwidth of FBG and the frequency detuning between the central wavelength of FBG and the lasing longitudinal mode on the chaotic bandwidth are investigated systematically, and the results demonstrate that the wavelength and bandwidth of the chaotic signal can be controlled to a certain extent through adjusting the related parameters of FBG.

(Received October 15, 2019; accepted October 22, 2020)

Keywords: Weak resonant-cavity Fabry-Perot laser diode (WRC-FPLD), Chaos signal, Wavelength tunability, Bandwidth controllability, Fiber Bragg grating (FBG), Filtered feedback

1. Introduction

Since chaos synchronization of complex systems was first demonstrated by Pecora and Carroll in 1990 [1], optical chaos and its applications have attracted extensive attention [2-23]. In particular, for the application of chaos in secure optical communication [8-23], many research groups have carried out a series of fruitful explorations, in which two significant investigations were that Van Wiggeren *et al.* reported a chaotic optical communication experiment in 1998 [8] and Argyris *et al.* conducted a field experiment of SL-based chaotic communication using a commercial fiber network in Athens in 2005 [9]. In optical chaotic communication systems, communication transmission capacity is one of the most concerned problems. In general, there are two ways to improve the transmission capacity of optical chaotic communication system, where one is to increase the single channel information transmission rate and the other is to adopt wavelength division multiplexing (WDM) technology. For the former, based on the nonlinear electro-optic phase dynamics, Lavrov *et al.* experimentally reported 10 Gbit/s single-channel long-distance optical chaotic communication in 2010 [10]. Based on the nonlinear dynamics of a modulator, Ke *et al.* experimentally demonstrated 30 Gbit/s signal over 100 km transmission through adopting duobinary modulation format in 2018 [11]. For the latter, some theoretical and experimental investigations have been explored on the WDM technology application in optical chaotic communication [19-23]. For example, Paul *et al.* experimentally

demonstrated two channels chaotic optical communication over a transmission path by using two external-cavity distributed feedback (DFB) semiconductor lasers (SLs) to generate dual-channel chaotic carriers [19]. Based on two pairs of Nd:YVO₄ microchip lasers operating at different wavelengths, Matsuura *et al.* initially realized one-way chaotic secure transmission of two-way information in WDM systems [20]. Zhang *et al.* theoretically studied WDM transmission of chaotic optical communication, and implemented a comparison between chaotic WDM optical communication and traditional WDM optical communication [21]. Even so, we have noticed that few experimental reports have been implemented on chaotic WDM optical communication above two channels so far. It is generally known that SLs are the most commonly used optical chaos sources since they are relatively easy to be driven into chaos under an external disturbance including optical feedback, optoelectronic feedback or optical injection [24-27]. For an SL-based chaotic WDM optical communication, wavelength tunability and bandwidth controllability of chaotic carriers are two key indicators, where the former can establish the desired wavelength channels and the latter can increase single-channel transmission rate and reduce the crosstalk among channels. Among different types of SLs, DFB-SLs have been widely used as chaotic sources, but their wavelength tunability is relatively poor. Compared with DFB-LD, Fabry-Perot laser diodes (FPLDs) possess better wavelength tunability due to weaker mode selection. Via a wavelength-selected optical feedback element, since a FPLD under optical feedback can oscillate at different

longitude mode, the central wavelength of the FPLD-based chaotic resource can be tuned within a relatively large range. Relative to the traditional FPLDs, the mode selection is weaker in weak-resonant-cavity Fabry-Perot laser diodes (WRC-FPLDs) due to their longer cavity length and lower front-end reflectivity [28-30]. As a result, the chaotic signal with larger tuned range can be generated by WRC-FPLDs. Recently, our group proposed and experimentally demonstrated a scheme for achieving a wavelength-tunable and bandwidth-controllable chaotic source [28] by combining a WRC-FPLD with a fiber Bragg grating (FBG), but related theoretical study is still lack.

Based on above considerations, in this paper, we propose a modified multi-mode rate equation model to characterize the chaotic dynamical system based on a WRC-FPLD subject to FBG feedback. The simulated results show that the wavelength of the chaotic signal can be adjusted through varying the central wavelength of FBG, and the chaotic bandwidth can be controlled by changing the feedback coefficient k , which is in agreement with our previous report [28]. Furthermore, we analyze the influences of the reflected bandwidth of FBG and the frequency detuning Δf between the central wavelength of FBG and the lasing longitudinal mode of the laser on the chaotic bandwidth.

2. Theory model

Based on the multi-mode rate equation model of SLs [31], further taking into account FBG feedback [32], the modified rate equations governing dynamics of the WRC-FPLD subject to FBG feedback can be described as follows:

$$\begin{aligned} \frac{dE_m(t)}{dt} = & \frac{1}{2}(1+i\alpha)[G_m(N) - \gamma]E_m(t) + \sqrt{2\beta N}\zeta_m(t) \\ & + k \sum_{m=1}^M E_m(t-\tau) \exp(-i2\pi f_m \tau) \\ & * r(t) \exp(i2\pi\Delta f_m t) \exp(i2\pi\Delta f t) \end{aligned} \quad (1)$$

$$\frac{dN(t)}{dt} = \gamma_e [CN_{th} - N(t)] - \sum_{m=1}^M G_m(N) |E_m(t)|^2 \quad (2)$$

where the subscript m corresponds to the m -th longitudinal mode of WRC-FPLD, M is the considered total mode number of WRC-FPLD. E is the slowly varied complex amplitude of the electric field, and $|E(t)|^2$ corresponds to the photon number. N , N_0 , and N_{th} are the carrier number, transparent carrier number and threshold carrier number, respectively. α is the line-width enhancement factor, γ is the cavity decay rate, γ_e is the carrier decay rate. k is the feedback coefficient, τ is the feedback delay time, C is the normalized current to the threshold current (C takes 1 at threshold). f_m is the m -th longitudinal mode frequency of the free running WRC-FPLD, and $\Delta f_m (= f_g - f_m$, where f_g is the Bragg frequency of FBG) is the frequency deviation

of the m -th mode from the Bragg frequency of FBG. The frequency detuning $\Delta f = f_g - f$, where f is the frequency of the mode nearest to the FBG. $*$ denotes convolution, $r(t)$ is the impulse response of the FBG. β is the spontaneous emission factor, and the spontaneous emission noise is represented by the Langevin noise $\zeta_m(t)$, which are assumed to be Gaussian white noise with unity intensity and zero mean. The mode-dependent optical gain is assumed to be a parabolic profile with a maximum centered at m_c -th mode, and it can be defined as:

$$G_m = \frac{g_c(N - N_0)}{1 + s \sum_m |E_m(t)|^2} [1 - (\frac{m - m_c}{\Delta f_g} \Delta f_L)^2] \quad (3)$$

where g_c is the differential gain factor, and s is the gain saturation parameter. Δf_L is the mode interval, Δf_g is the gain bandwidth of the gain material.

The impulse response of the FBG $r(t)$ is given by the inverse Fourier transform of the frequency response of the FBG:

$$r(\Omega) = \frac{k_B^2 \sinh(\sqrt{k_B^2 - \delta^2} L)}{-\delta \sinh(\sqrt{k_B^2 - \delta^2} L) + i\sqrt{k_B^2 - \delta^2} \cosh(\sqrt{k_B^2 - \delta^2} L)} \quad (4)$$

where k_B is the magnitude of the coupling coefficient of the FBG. δ represents the phase mismatch between the counter-propagating modes and equals to $n_g \Omega / c$, where n_g is the group index of the fiber and c is the speed of light in vacuum. L is the length of the FBG. For simplicity, a single-mode uniform FBG is assumed, whose reflection bandwidth can be approximated by $ck_B / \pi n_g$.

3. Results and discussion

Above multi-mode rate equations can be solved by adopting fourth-order Runge-Kutta algorithm. During the calculations, the used parameters are set as follows [33], [34]: $a = 6$, $\gamma = 4.3 \times 10^2 \text{ ns}^{-1}$, $\gamma_e = 1 \text{ ns}^{-1}$, $\beta = 5 \times 10^{-7} \text{ ns}^{-1}$, $N_0 = 7.3 \times 10^7$, $N_{th} = 2.1 \times 10^8$, $g_c = 3.2 \times 10^{-6} \text{ ns}^{-1}$, $s = 1.0 \times 10^{-7}$, $\Delta f_L = 70 \text{ GHz}$, $\Delta f_g = 1.4 \times 10^4 \text{ GHz}$, $\tau = 4 \text{ ns}$, $C = 2$, $n_g = 1.45$, $L = 20 \text{ mm}$. The total mode number M in a free-running WRC-FPLD is assumed to be 21 after considering the computing ability of the computer.

Fig. 1 shows the optical spectrum of a free-running WRC-FPLD. For convenience of description, the main lasing mode located at 1550.24 nm is marked as "11-th mode", and the other modes are marked as from "10-th mode" to "1-th mode" in the short-wave direction, and from "12-th mode" to "21-th mode" in the long-wave direction, respectively. The longitudinal modes distribution profile is not a strict Lorentz line due to the noise.

After introducing a FBG filtered feedback, different modes will experience different losses. In particular, when the reflected bandwidth of FBG is smaller than the mode interval and meanwhile the filtered feedback is strong enough, only one longitudinal mode oscillates. As a result, by varying the Bragg wavelength of the FBG, different

longitudinal mode can be chosen to become a lasing mode. Here, we take the cases that the Bragg wavelength of the FBG is respectively identical to the oscillated wavelength of “13-th mode”~“9-th mode” as examples. Fig. 2 shows the time series (first column), power spectra (second column) and optical spectra (third column) of the WRC-FPLD subject to FBG filtered feedback with a feedback coefficient $k = 6 \text{ ns}^{-1}$. Here, k_B of FBG takes 100 m^{-1} , and the corresponding reflected bandwidth is 6.6 GHz, which

is smaller than the mode interval of the free running WRC-FPLD. As shown in this diagram, by adjusting the Bragg wavelength of FBG, different mode can be individually stimulated with a side-mode suppression rates (SMSR) of $>30 \text{ dB}$. Moreover, under $k = 6 \text{ ns}^{-1}$, the time series and power spectra demonstrate that these selected modes have been driven into the chaotic states.

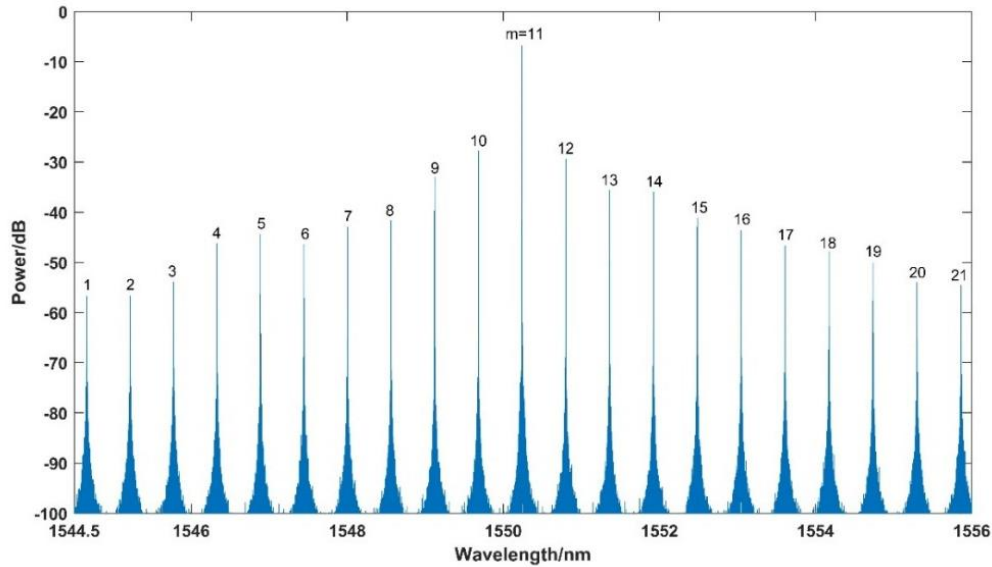


Fig. 1. Optical spectrum of a free running WRC-FPLD, where the 11-th mode is the main lasing mode located at 1550.24 nm (color online)

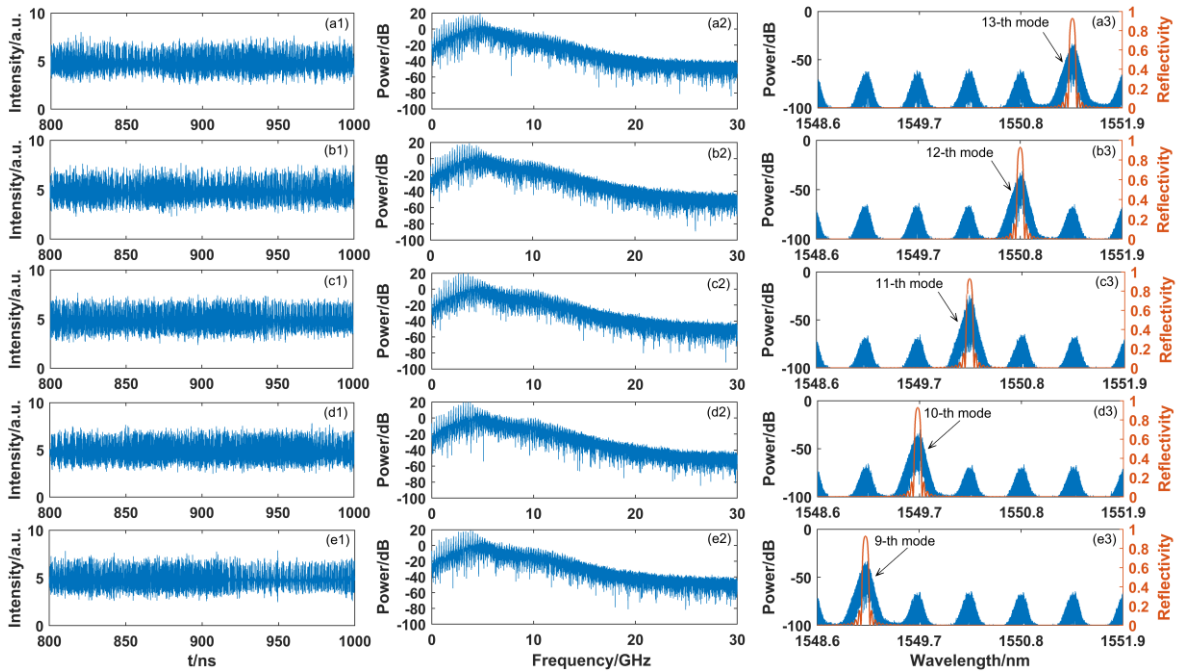


Fig. 2. Time series (Column 1), power spectra (Column 2) and optical spectra (Column 3) of the WRC-FPLD subject to FBG filtered feedback, where the Bragg wavelength of FBG equals to the wavelength of “13-th mode” (Row a), “12-th mode” (Row b), “11-th mode” (Row c), “10-th mode” (Row d) and “9-th mode” (Row e) of the free running WRC-FPLD, respectively, where the orange lines in the column 3 are the reflection spectra of FBG. The feedback coefficient $k = 6 \text{ ns}^{-1}$, $k_B = 100 \text{ m}^{-1}$ (corresponding reflected bandwidth of the FBG is 6.6 GHz), $\Delta f = 0$ (color online)

Next, we analyze the influence of the feedback coefficient k on the chaotic bandwidth of power spectrum. Here, the bandwidth is the standard bandwidth estimated as the span between DC and the frequency in which contains 80% of the energy. We take the case that the Bragg wavelength of the FBG λ_B is equal to the wavelength of the 12-th mode ($=1550.80$ nm) as an example. Fig. 3 displays the time series, power spectra and optical spectra of the WRC-FPLD subject to filtered feedback provided by the FBG with $k_B = 100$ m⁻¹ and different feedback coefficient k . For $k = 0$ (first row), the WRC-FPLD is at free-running, the time series (Fig. 3 (c1)) shows almost a constant value with small fluctuations due to the noise, and therefore the dynamic state is the stable state. For $k = 6$ ns⁻¹ (second row), the 12-th mode obtains more feedback power to become the lasing mode while the other modes are suppressed due to mode competition. The time series (Fig. 3 (a2)) exhibits relatively large fluctuations, the power spectrum (Fig. 3 (b2)) is continuous and enhanced within 0-10 GHz, and the optical

spectrum (Fig. 3 (c2)) is obviously broadened. As a result, the laser is driven into a chaotic state, and the chaotic bandwidth is about 5.0 GHz. For $k = 40$ ns⁻¹ (third row), the optical spectrum (Fig. 3 (c3)) is further broadened, and an additional peak appears in the optical spectrum. Correspondingly, a peak around 12.2 GHz is observed in the power spectrum (Fig. 3 (b3)), which corresponds the frequency interval between the two peaks existing in the optical spectrum. Under this case, the bandwidth of chaotic output is expanded to about 12.3 GHz. For $k = 100$ ns⁻¹, the optical spectrum (Fig. 3 (c4)) is significantly broadened, and the frequency interval between the two peaks in optical spectrum is 20.5 GHz. Meantime, as shown in Fig. 3 (b4), the powers of high-frequency components increase, and the bandwidth of chaotic output reaches 20.9 GHz. For $k = 180$ ns⁻¹ (fifth row), as shown in Fig. 3 (c5), the 13-th mode is enhanced and the SMSR decreases, the time series and the power spectrum show the dynamic state is a quasi-period state, and the bandwidth is about 1.3 GHz.

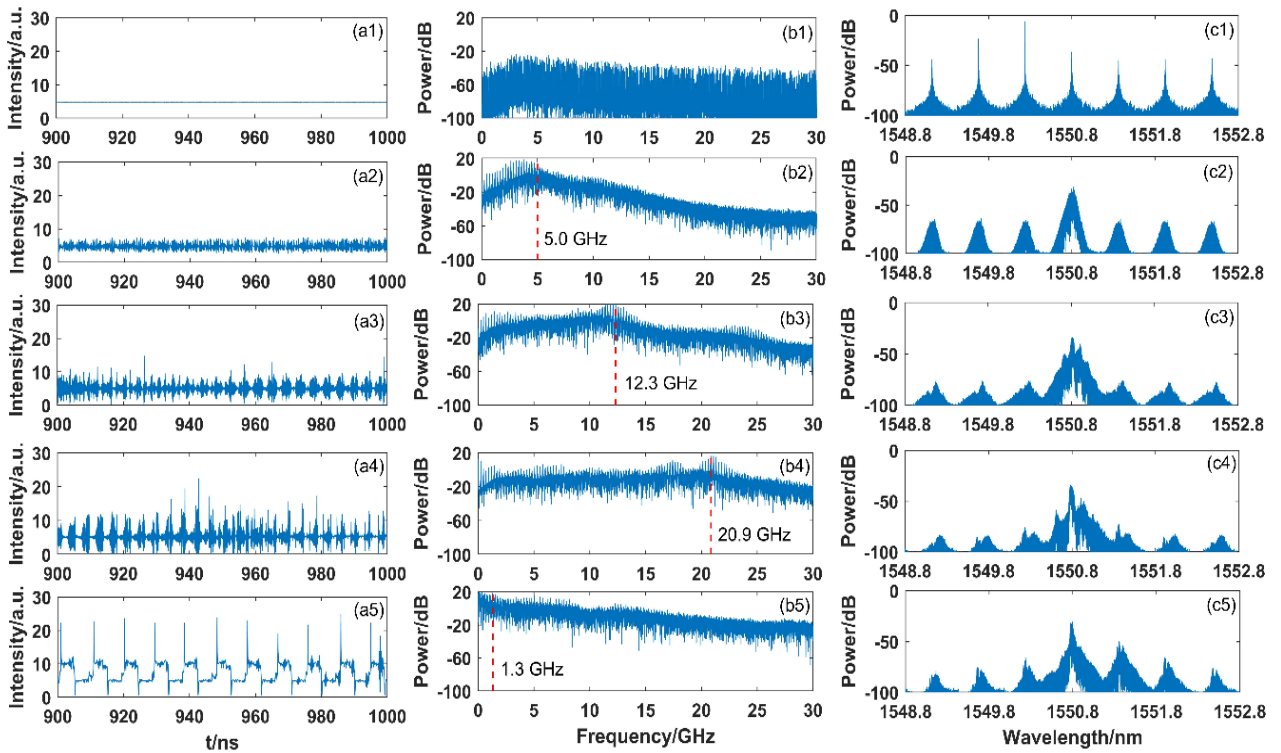


Fig. 3. Time series (Column a), power spectra (Column b) and optical spectra (Column c) of the output from WRC-FPLD under the feedback coefficient $k = 0$ (Row 1), 6 ns⁻¹ (Row 2), 40 ns⁻¹ (Row 3), 100 ns⁻¹ (Row 4), and 180 ns⁻¹ (Row 5), respectively, where $k_B = 100$ m⁻¹ (corresponding reflected bandwidth of FBG is 6.6 GHz), $\Delta f = 0$ and the Bragg wavelength of FBG is same as the wavelength of “12-th mode” of free running WRC-FPLD (color online)

To further illuminate the influence of the feedback coefficient k on the bandwidth of the chaos output from the WRC-FPLD subject to FBG filtered feedback, Fig. 4 gives the evolution of the chaotic bandwidth with k under different mode selected to be the lasing mode. From this diagram, it can be seen that the evolution trends are similar for three cases. Once k is more than 6 ns⁻¹, the WRC-FPLD can be driven into chaotic state under filter

feedback, and the bandwidths gradually increase with the increase of k . However, for $k > 170$ ns⁻¹, the bandwidth decreases suddenly. Through observing corresponding power spectra and optical spectra, we find that, under $k > 170$ ns⁻¹, the state of the WRC-FPLD is not a chaotic state due to too strong optical feedback. It should be pointed out that the sudden decrease of the bandwidth has not been observed in the experimental investigation [28], which

may be due to that the feedback strength is not enough strong in the experiment.

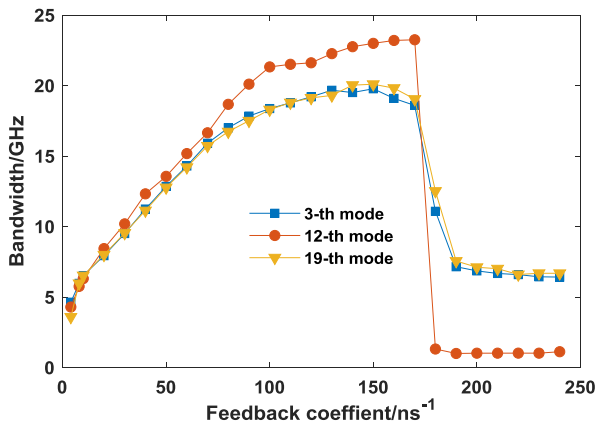


Fig. 4. Bandwidths of the chaotic outputs as a function of feedback coefficient k under three different longitudinal modes selected to be the lasing modes, respectively, where $k_B = 100 \text{ m}^{-1}$ and the corresponding reflected bandwidth of FBG is 6.6 GHz, $\Delta f = 0$ (color online)

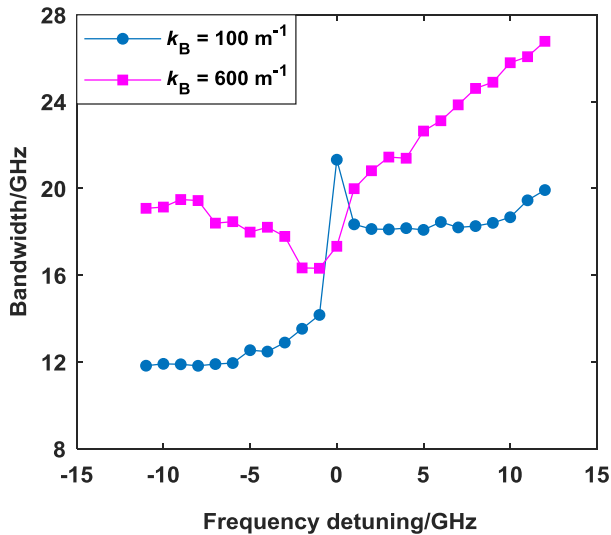


Fig. 5. Bandwidth of the "12-th mode" chaotic signal as a function of the frequency detuning Δf under $k = 100 \text{ ns}^{-1}$, where $k_B = 100 \text{ m}^{-1}$ (circles) and 600 m^{-1} (squares) (corresponding reflected bandwidth of FBG is 6.6 GHz and 40 GHz, respectively) (color online)

The above results demonstrate that the chaotic bandwidth is seriously affected by the feedback coefficient k . Finally, we will analyze the influences of the frequency detuning Δf and the reflected bandwidth of FBG on the chaotic bandwidth. The bandwidth evolutions with Δf under different reflected bandwidth of FBG are presented in Figure 5, where $k = 100 \text{ ns}^{-1}$ and the 12-th mode is chosen as an example. The value of k_B takes 100 m^{-1} (circles) and 600 m^{-1} (squares), and corresponding reflected bandwidth of FBG is 6.6 GHz and 40 GHz, respectively. From this diagram, on one hand, a positive frequency detuning is more helpful for generating a chaotic signal with a larger bandwidth, which is accord

with the result in Ref. [33]. On the other hand, different evolutionary trends of the chaotic bandwidth can be observed for different k_B . For $k_B = 100 \text{ m}^{-1}$, the chaotic bandwidth arrives at its maximum when $\Delta f = 0$. With the increase of $|\Delta f|$, the chaotic bandwidth gradually decreases. Such an evolutionary trends may be due to a joint action of the oscillated wavelength red-shift resulted by optical feedback and the wavelength-selective optical feedback provided by FBG, and the influence of the FBG reflected sideband is not obvious since the peak of reflected sideband is below 0.2. However, for $k_B = 600 \text{ m}^{-1}$, the peak of FBG reflected sideband is increased to 0.8. After overlaying the effect resulted by the strong reflected sideband, the evolutionary trend of the chaotic bandwidth with Δf behaves more complicated. For $\Delta f = 12 \text{ GHz}$, the chaotic bandwidth arrives at its maximum (about 26.8 GHz). However, once $|\Delta f|$ exceeds 12 GHz, the adjacent longitudinal mode will be stimulated, and then single longitudinal mode operation cannot be achieved for the WRC-FPLD.

4. Conclusions

In summary, for our previously reported experimental results on the chaotic output characteristics of a weak resonant-cavity Fabry-Perot laser diode (WRC-FPLD) subject to fiber Bragg grating (FBG) filtered feedback [28], we present a numerical investigation by using a modified multi-mode rate equation model in this work. The results show that, by adjusting the Bragg frequency of FBG and choosing an appropriate feedback coefficient k , different longitudinal mode can be chosen to become a lasing mode operating at a chaotic state, and the bandwidth of the chaotic output is firstly increased and then decreased with the increase of k . Such a variation trend is consistent with our experimentally reported in [28]. Moreover, the effects of the FBG reflected bandwidth and the frequency detuning Δf between the central wavelength of FBG and the lasing longitudinal mode on the chaotic bandwidth have been analyzed. By selecting suitable feedback parameters, wavelength-tunable and bandwidth-controllable chaotic signals can be obtained based on a WRC-FPLD subject to FBG feedback.

Acknowledgments

This research was funded by the National Natural Science Foundation of China (Grant Nos. 61475127, 61575163, 61775184, and 61875167).

References

- [1] L. M. Pecora, T. L. Carrol, Phys. Rev. Lett. **64**(8), 821 (1990).
- [2] J. Mork, B. Trombory, J. Mark, IEEE J. Quantum Electron. **28**(1), 93 (1992).

- [3] J. F. Liao, J. Q. Sun, *Opt. Commun.* **295**, 188 (2013).
- [4] M. Sciamanna, K. A. Shore, *Nature Photonics* **9**, 151 (2015).
- [5] F. Y. Lin, J. M. Liu, *IEEE J. Quantum Electron* **40**(6), 815 (2004).
- [6] D. Z. Zhong, G. L. Xu, W. Luo, Z. Z. Xiao, *Opt. Express* **25**(18), 21684 (2017).
- [7] X. Tang, G. Q. Xia, C. Ran, T. Deng et al., *IEEE Photonics J.* **11**(2), 7800710 (2019).
- [8] G. D. VanWiggeren, R. Roy, *Science* **279**(5354), 1198 (1998).
- [9] A. Argyris, D. Syvridis, L. Larger et al., *Nature* **438**(17), 343 (2005).
- [10] R. Lavrov, M. Jacquot, L. Larger, *IEEE J. Quantum Electron.* **46**(10), 1430 (2010).
- [11] J. X. Ke, L. L. Yi, G. Q. Xia, W. S. Hu, *Opt. Lett.* **43**(6), 1323 (2018).
- [12] D. R. Frey, *IEEE Trans. Circuits Syst. II Analog Digit. Signal Process* **40**(10), 660 (1993).
- [13] J. M. Liu, H. F. Chen, S. Tang, *IEEE J. Quantum Electron.* **38**(9), 1184 (2002).
- [14] J. Ohtsubo, *IEEE J. Quantum Electron.* **38**(9), 1141 (2002).
- [15] S. Tang and J. Liu, *Phys. Rev. Lett.* **90**(19), 194101 (2003).
- [16] J. M. Buldu, J. Garcia-Ojalvo, M. C. Torrent, *IEEE J. Quantum Electron.* **40**(6), 640 (2004).
- [17] G. H. Li, A. B. Wang, Y. Feng, et al., *Chin. Phys. B* **19**(7), 070515 (2010).
- [18] J. G. Wu, Z. M. Wu, X. Tang et al., *IEEE Photonics Technol. Lett.* **25**(6), 587 (2013).
- [19] J. Paul, S. Sivaraman, K. A. Shore, *J. Opt. Soc. Am. B* **21**(3), 514 (2004).
- [20] T. Matsuura, A. Uchida, S. Yoshimori, *Opt. Lett.* **29**(23), 2731 (2004).
- [21] J. Z. Zhang, A. B. Wang, J. F. Wang et al., *Opt. Express* **17**(8), 6357 (2009).
- [22] A. Argyris, E. Grivas, A. Bogris et al., *J. Lightwave Technol.* **28**(21), 3107 (2010).
- [23] N. Jiang, C. P. Xue, Y. X. Lv, et al., *Nonlinear Dyn.* **86**, 1937 (2016).
- [24] F. Rogister, A. Locquet., *Opt. Lett.* **26**(19), 1486 (2011).
- [25] H. D. I. Abarbanel, M. B. Kennel et al., *IEEE J. Quantum Electron.* **37**(10), 1301 (2001).
- [26] J. Liu, Z. M. Wu, G. Q. Xia, *Opt. Express* **17**(15), 12619 (2009).
- [27] J. J. Chen, Y. N. Duan, L. F. Li, et al., *IEEE Access* **6**, 66807 (2018).
- [28] Z. Q. Zhong, G. R. Lin, Z. M. Wu et al., *IEEE Photonics Technol. Lett.* **29**(17), 1506 (2017).
- [29] M. Xu, Y.-C. Chi, J. Wang, L. Cheng, F. Lu, M. I. Khalil et al., *IEEE Photonics Technol. Lett.* **27**(17), 1821 (2015).
- [30] M. L. Deng, R. P. Giddings, C.-T. Tsai, G.-R. Lin, J. M. Tang, *IEEE Photonics Technol. Lett.* **30**(1), 43 (2018).
- [31] M. Yousefi, A. Barsella, D. Lenstra, G. Morthier et al., *IEEE J. Quantum Electron.* **39**(10), 1229 (2003).
- [32] S. S. Li, S. C. Chan, *IEEE J. Sel. Top. Quantum Electron.* **21**(6), 100812 (2015).
- [33] S.-Y. Lin, Y.-C. Chi, Y.-C. Su, Y.-C. Li, G.-R. Lin, *IEEE Photonics J.* **7**(1), 7200309 (2015).
- [34] Q. Yang, Z. M. Wu, J. G. Wu, G. Q. Xia, *Opt. Commun.* **281**, 5025 (2008).

*Corresponding author: zmwu@swu.edu.cn